Thickness of graphene and single-wall carbon nanotubes

Y. Huang,[1,*] J. Wu,[2] and K. C. Hwang[2]
[1]*Department of Mechanical Science and Engineering, University of Illinois, Urbana, Illinois 61801, USA*
[2]*FML, Department of Engineering Mechanics, Tsinghua University, Beijing 10084, China*
(Received 11 August 2006; published 12 December 2006)

Young's modulus and the thickness of single wall carbon nanotubes (CNTs) obtained from prior atomistic studies are largely scattered. In this paper we establish an analytic approach to bypass atomistic simulations and determine the tension and bending rigidities of graphene and CNTs directly from the interatomic potential. The thickness and elastic properties of graphene and CNTs can also be obtained from the interatomic potential. But the thickness, and therefore elastic moduli, also depend on type of loading (e.g., uniaxial tension, uniaxial stretching, equibiaxial stretching), as well as the nanotube radius R and chirality when $R<1$ nm. This explains why the thickness obtained from prior atomistic simulations is scattered. This analytic approach is particularly useful in the study of multiwall CNTs since their stress state may be complex even under simple loading (e.g., uniaxial tension) due to the van der Waals interactions between nanotube walls. The present analysis also provides an explanation of Yakobson's paradox that the very high Young's modulus reported from the atomistic simulations together with the shell model may be due to the not-well-defined CNT thickness.

DOI: 10.1103/PhysRevB.74.245413 PACS number(s): 61.46.Fg, 46.70.De, 62.25.+g, 81.07.De

I. INTRODUCTION

Numerous atomistic and continuum studies have shown that carbon nanotubes (CNTs) possess high Young's modulus on the order of 1 TPa, which is $5\sim6$ times stiffer than steel.[1–16] However, atomistic studies of single-wall CNTs, such as molecular dynamic simulations based on the empirical interatomic potential,[17,18] tight-binding model,[19] and density functional theory,[20] can determine the stiffness Eh of single-wall CNTs which is the product of Young's modulus E and nanotube thickness h. One needs to assume a thickness h for single-wall CNTs in order to determine their Young's modulus from atomistic studies, even though it is ambiguous to define the thickness for a single layer of atoms. One approach is to take the interlayer spacing of graphite $h=0.34$ nm as the CNT thickness.[6,7,10,15,21] Such a thickness, however, is an order of magnitude larger than other results shown in Table I.

Another approach is to model single-wall CNTs as linear elastic thin shells.[4,12,14,22–28] Young's modulus E and the shell thickness h are determined by fitting the atomistic simulation results of tensile rigidity $Eh/(1-\nu^2)$ and bending rigidity $Eh^3/[12(1-\nu^2)]$ of single-wall CNTs, where ν is Poisson's ratio. Such an approach gives the CNT thickness h much smaller than the graphite interlayer spacing (0.34 nm), ranging from 0.06 to 0.09 nm (Table I). The scattered CNT thickness ($0.06\sim0.09$ nm) depends on the interatomic potential as well as simulation details.

Why is the CNT thickness so scattered? Is it possible to link the CNT thickness directly to the interatomic potential? The objective of this paper is to establish an *analytic* method that bypasses atomistic simulations, and determines the tension and bending rigidities of single-wall CNTs directly from the interatomic potential. Analytical expressions of tension and bending rigidities are obtained in terms of parameters in the interatomic potential. The analytic expressions clearly show the importance of multibody atomistic interactions, without which the CNTs would have had no bending rigidity. The CNT thickness could be defined from the tension and bending rigidities as in some prior work,[4,12,14,22–28] but such thickness is not strictly a constant for each interatomic potential. Instead, it also depends on the type of loading the CNT is subject to (e.g., uniaxial tension, uniaxial stretching, biaxial stretching). For uniaxial tension, the CNT thickness is around 0.06 nm, but it becomes approximately 0.09 nm for equibiaxial stretching. This range ($0.06\sim0.09$ nm) given by the analytic expression is the same as that reported by atomistic simulations and continuum shell models shown in Table I.

The paper is outlined as follows. We briefly describe the formulation of multibody interatomic potentials for carbon in Sec. II, and identify parameters in the interatomic potential that govern the tension and bending rigidities of CNTs. The proposed analytical approach is shown in Sec. III for an arbitrary interatomic potential. The CNT thickness, defined from the tension and bending rigidities,[4,12,14,22–24] are obtained in Sec. IV, but is shown to depend on the type of loading. Specific results are given for the Brenner potential[17] and its second-generation potential[18] in Sec. V. A discussion in view of "Yakobson's paradox"[33] is given in Sec. VI.

II. FORMULATION OF MULTIBODY INERATOMIC POTENTIALS FOR CARBON

There are many interatomic potentials for carbon.[17,18,34,35] They can be generally written as

$$V=V(r_{ij};\theta_{ijk},k\neq i,j)=V(r_{ij};\cos\theta_{ijk},k\neq i,j) \quad (2.1)$$

for a pair of atoms i and j, where r_{ij} is the bond length, θ_{ijk} is the bond angle between $i-j$ and $i-k$ bonds, and $k(\neq i,j)$ represents atoms in the vicinity. The θ_{ijk} term, or equivalently, $\cos\theta_{ijk}$ term, represents the multibody atomistic interactions in carbon. For the unstrained equilibrium state (i.e., strain $\varepsilon=0$), the equilibrium bond length and angle are denoted by $(r_{ij})_0$ and $(\cos\theta_{ijk})_0$, respectively.

TABLE I. The thickness and Young's modulus of carbon nanotubes.

Authors	Method	Wall thickness (nm)	Young's modulus (TPa)
Lu[a]	Molecular dynamics	0.34	0.974
Hernández *et al.*[b]	Tight binding molecular dynamics	0.34	1.24
Odegard *et al.*[c]	Equivalent-continuum modeling	0.69	
Li and Chou[d]	Structural mechanics: stiffness matrix method	0.34	1.01
Jin and Yuan[e]	Molecular dynamics	0.34	1.238
Tserpes and Papanikos[f]	Structural mechanics: FE method	0.147	
Yakobson *et al.*[g]	Molecular dynamics	0.066	5.5
Zhou *et al.*[h]	Tight-binding model	0.074	5.1
Kudin *et al.*[i]	*Ab inito* computations	0.089	3.859
Tu and Ou-yang[j]	Local density approximation model	0.075	4.7
Vodenitcharova and Zhang[k]	Ring theory continuum mechanics	0.0617	4.88
Panatano *et al.*[l]	Continuum shell modeling	0.075	4.84
Goupalov[m]	Continuum model for long-wavelength phonons	0.087	
Wang *et al.*[n]	Ab *initio* calculation	0.0665	5.07

[a]Reference 6.
[b]Reference 7.
[c]Reference 29.
[d]Reference 21.
[e]Reference 15.
[f]Reference 30.
[g]Reference 4.
[h]Reference 12.
[i]Reference 14.
[j]Reference 22.
[k]Reference 31.
[l]Reference 23.
[m]Reference 32.
[n]Reference 24.

For an infinitesimal strain $\boldsymbol{\varepsilon}$, the changes of bond length $r_{ij}-(r_{ij})_0$ and bond angle $\theta_{ijk}-(\theta_{ijk})_0$ are also infinitesimal such that the interatomic potential in Eq. (2.1) can be expanded to the Taylor series. We use graphene as an example to illustrate this. The bond angle for graphene at the unstrained, equilibrium state is $(\theta_{ijk})_0=120°$. The equilibrium bond length r_0 is determined by minimizing the potential V at the fixed bond angle 120°, i.e.,

$$\left.\frac{\partial V}{\partial r_{ij}}\right|_{r_{ij}=r_0,\theta_{ijk}=120^o}=0.$$

For an infinitesimal strain $\boldsymbol{\varepsilon}$, $r_{ij}-r_0$ and $\cos\theta_{ijk}+\frac{1}{2}$ are also infinitesimal.

The Taylor expansion of Eq. (2.1) for graphene becomes

$$V=V_0+\sum_{k\neq i,j}\left(\frac{\partial V}{\partial\cos\theta_{ijk}}\right)_0\left(\cos\theta_{ijk}+\frac{1}{2}\right)+\frac{1}{2}\left(\frac{\partial^2 V}{\partial r_{ij}^2}\right)_0(r_{ij}-r_0)^2+\sum_{k\neq i,j}\left(\frac{\partial^2 V}{\partial r_{ij}\partial\cos\theta_{ijk}}\right)_0(r_{ij}-r_0)\left(\cos\theta_{ijk}+\frac{1}{2}\right)$$
$$+\frac{1}{2}\sum_{k,l\neq i,j}\left(\frac{\partial^2 V}{\partial\cos\theta_{ijk}\partial\cos\theta_{ijl}}\right)_0\left(\cos\theta_{ijk}+\frac{1}{2}\right)\left(\cos\theta_{ijl}+\frac{1}{2}\right),\tag{2.2}$$

where the subscript "0" denotes the values at the unstrained equilibrium state, $r_{ij}=r_0$ and $\theta_{ijk}=120°$; and the terms higher than the second order are neglected since they do not contribute to the tension and bending rigidities which are defined at the infinitesimal strain. The first-order derivative $(\partial V/\partial r_{ij})_0$ vanishes and therefore does not appear in the Taylor expansion (2.2), which involves five constants of the interatomic potential, namely the first-order derivative

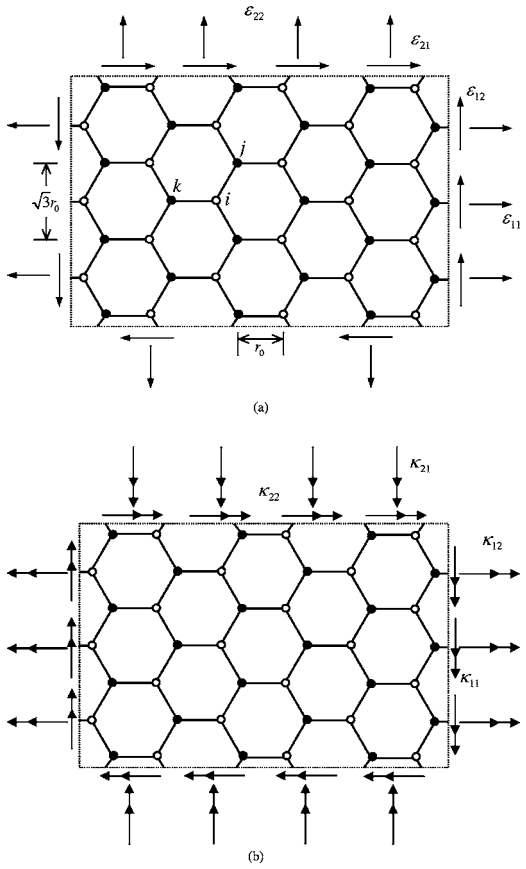

FIG. 1. A schematic diagram of a graphene subject to (a) in-plane strain and (b) curvature.

$(\partial V/\partial \cos\theta_{ijk})_0$, and second-order derivatives $(\partial^2 V/\partial r_{ij}^2)_0$, $(\partial^2 V/\partial r_{ij}\partial \cos\theta_{ijk})_0$, $(\partial^2 V/\partial \cos\theta_{ijk}\partial \cos\theta_{ijk})_0$, and $(\partial^2 V/\partial \cos\theta_{ijk}\partial \cos\theta_{ijl})_0 (k\neq l)$. These five constants evaluated at the unstrained equilibrium state ($\boldsymbol{\varepsilon}=0$) can be analytically obtained for any interatomic potential. The tension and bending rigidities are given in terms of these five constants in Sec. III for any interatomic potential, while the thickness is given in Sec. IV. Results are presented for two specific potentials[17,18] in Sec. V. For the Brenner potential,[17] the above five constants are given analytically in the Appendix in terms of parameters in the potential, and they are 1.841 eV, 4337 eV nm^{-2}, −49.49 eV nm^{-1}, 3.014 eV and −0.3728 eV, respectively, and the equilibrium bond length determined analytically from $(\partial V/\partial r_{ij})_0=0$ in terms of parameters in the potential, and is $r_0=0.145$ nm. For its second-generation potential,[18] these five constants and r_0 become 1.592 eV, 4356 eV nm^{-2}, −59.14 eV nm^{-1}, 3.099 eV, −0.3673 eV, and 0.142 nm, respectively.

It is important to note that, even though the first-order derivative $(\partial V/\partial r_{ij})_0=0$ at the unstrained, equilibrium state, the other first-order derivative $(\partial V/\partial \cos\theta_{ijk})_0$ does not vanish and it reflects the multibody atomistic interactions. In fact, as to be seen in Sec. III and IV, the graphene bending rigidity and therefore thickness all result from the nonvanishing $(\partial V/\partial \cos\theta_{ijk})_0$.

III. TENSION AND BENDING RIGIDITIES OF GRAPHENE

We first study a graphene subject to uniform in-plane normal strains ε_{11} and ε_{22} and shear strain ε_{12}, as shown in Fig. 1(a). It is important to note that the atom positions become nonuniform even for a uniform strain because graphene does not have a simple Bravais lattice. Zhang *et al.*[36,37] developed a simple, analytic method to determine atom positions by decomposing the atomic structure of graphene to two simple Bravais sublattices [marked by open and solid circles in Fig. 1(a)]. A shift vector between two sublattices was introduced to ensure the equilibrium of atoms by minimizing energy with respect to the shift vector for each given strain $\boldsymbol{\varepsilon}$. The distance r_{ij} between two nearest-neighbor atoms [from *different* sublattices marked by open and closed circles in Fig. 1(a)] is given by $r_{ij}{}^2=r_0{}^2(\delta_{\alpha\beta}+2\varepsilon_{\alpha\beta})(n_\alpha+x_\alpha)(n_\beta+x_\beta)$, where r_0 and $\mathbf{n}$ are the bond length and directions prior to deformation, $\delta_{\alpha\beta}$ is the second-order identity tensor, and $\mathbf{x}=\mathbf{x}(\boldsymbol{\varepsilon})$ is the shift vector (normalized by r_0) to be determined analytically via energy minimization.

We now consider the graphene subject to combined in-plane strain $\varepsilon_{\alpha\beta}$ $(\alpha,\beta=1,2)$ and curvature κ_{11}, κ_{22}, and κ_{12} (Fig. 1), which cause stretching and bending of the graphene, respectively. The distance between two nearest-neighbor atoms (from *different* sublattices) now becomes

$$r_{ij}^2 = r_0^2(\delta_{\alpha\beta}+2\varepsilon_{\alpha\beta})(n_\alpha+x_\alpha)(n_\beta+x_\beta) - r_0^4[\kappa_{\alpha\beta}(n_\alpha+x_\alpha)(n_\beta+x_\beta)]^2/12, \tag{3.1}$$

where the first term on the right hand side is due to the in-plane strain, and the second term represents the bond length reduction due to the curvature; the shift vector $\mathbf{x}=\mathbf{x}(\boldsymbol{\varepsilon},\boldsymbol{\kappa})$ is to be determined analytically via energy minimization. The bond angle θ_{ijk} between bonds $i-j$ and $i-k$ can be similarly obtained as

$$\cos\theta_{ijk} = \frac{r_0^2}{r_{ij}r_{ik}}(n_\alpha^{(1)}+x_\alpha)(n_\lambda^{(2)}+x_\lambda)\left\{\delta_{\alpha\lambda}+2\varepsilon_{\alpha\lambda}+\frac{r_0^2}{12}\kappa_{\alpha\beta}\kappa_{\gamma\lambda}\times[3(n_\beta^{(1)}+x_\beta)(n_\gamma^{(2)}+x_\gamma)-2(n_\beta^{(2)}+x_\beta)(n_\gamma^{(2)}+x_\gamma) - 2(n_\beta^{(1)}+x_\beta)(n_\gamma^{(1)}+x_\gamma)]\right\}, \tag{3.2}$$

where $\mathbf{n}^{(1)}$ and $\mathbf{n}^{(2)}$ represent the directions of $i-j$ and $i-k$ bonds prior to deformation, respectively.

The substitution of Eqs. (3.1) and (3.2) into the Taylor expansion (2.2) gives the bond energy V as a quadratic function of strain $\boldsymbol{\varepsilon}$, shift vector $\mathbf{x}$, and curvature $\boldsymbol{\kappa}$. The energy associated with each atom is $\Phi=\frac{1}{2}\Sigma_{j=1}^3 V(r_{ij};\cos\theta_{ijk},k\neq i,j)$, where the summation is for three nearest-neighbor atoms, and the factor one half results from the equipartition of bond energy. The shift vector is determined from energy minimization $\partial\Phi/\partial x_\lambda=0$ as

$$x_\lambda = \frac{2}{3}A\varepsilon_{\alpha\beta}\sum_{j=1}^{3} n_\alpha n_\beta n_\lambda, \tag{3.3}$$

which depends on the in-plane strain $\boldsymbol{\varepsilon}$ but not curvature $\boldsymbol{\kappa}$, and

$$A = 1 - \frac{8r_0^2\left(\frac{\partial^2 V}{\partial r_{ij}^2}\right)_0 + 12r_0\left(\frac{\partial^2 V}{\partial r_{ij}\partial \cos\theta_{ijk}}\right)_0}{12\left(\frac{\partial V}{\partial \cos\theta_{ijk}}\right)_0 + 4r_0^2\left(\frac{\partial^2 V}{\partial r_{ij}^2}\right)_0 + 18\left(\frac{\partial^2 V}{\partial \cos\theta_{ijk}\partial \cos\theta_{ijk}}\right)_0 - 9\left(\frac{\partial^2 V}{\partial \cos\theta_{ijk}\partial \cos\theta_{ijl}}\right)_0 + 12r_0\left(\frac{\partial^2 V}{\partial r_{ij}\partial \cos\theta_{ijk}}\right)_0}. \quad (3.4)$$

All five derivatives of the interatomic potential and the equilibrium bond length r_0 come into play.

The strain energy density (energy per unit area of graphene), $\Phi/(3\sqrt{3}r_0^2/4)$, becomes a quadratic function of $\boldsymbol{\varepsilon}$ and $\boldsymbol{\kappa}$ once the shift vector $\mathbf{x}$ is substituted by Eq. (3.3). The stress is the work conjugate of strain, and is given by

$$(\sigma_{11}+\sigma_{22})h = \frac{1}{\sqrt{3}}\left(\frac{\partial^2 V}{\partial r_{ij}^2}\right)_0 (\varepsilon_{11}+\varepsilon_{22}),$$

$$\begin{Bmatrix} (\sigma_{11}-\sigma_{22})h \\ \sigma_{12}h \end{Bmatrix} = \frac{B}{8\sqrt{3}}\begin{Bmatrix} \varepsilon_{11}-\varepsilon_{22} \\ \varepsilon_{12} \end{Bmatrix}, \quad (3.5)$$

where the stress appears together with the "thickness" h of graphene since the strain energy density is the energy per unit area (instead of volume); and

$$B = \frac{3(1-A)^2}{r_0^2}\left[4\left(\frac{\partial V}{\partial \cos\theta_{ijk}}\right)_0 + 6\left(\frac{\partial^2 V}{\partial \cos\theta_{ijk}\partial \cos\theta_{ijk}}\right)_0 - 3\left(\frac{\partial^2 V}{\partial \cos\theta_{ijk}\partial \cos\theta_{ijl}}\right)_0\right] + 4(1+A)^2\left(\frac{\partial^2 V}{\partial r_{ij}^2}\right)_0 - 12\frac{(1-A^2)}{r_0}\left(\frac{\partial^2 V}{\partial r_{ij}\partial \cos\theta_{ijk}}\right)_0. \quad (3.6)$$

The shear rigidity (ratio of $\sigma_{12}h$ to ε_{12}) is proportional to B, and the biaxial tension rigidity [ratio of $(\sigma_{11}+\sigma_{22})h$ to $(\varepsilon_{11}+\varepsilon_{22})$] is proportional to $(\partial^2 V/\partial r_{ij}^2)_0$. On the other hand, the classical plane-stress linear elastic relation[38] is

$$\sigma_{11}+\sigma_{22} = \frac{E}{1-\nu}(\varepsilon_{11}+\varepsilon_{22})$$

and

$$\begin{Bmatrix} \sigma_{11}-\sigma_{22} \\ \sigma_{12} \end{Bmatrix} = 2\mu\begin{Bmatrix} \varepsilon_{11}-\varepsilon_{22} \\ \varepsilon_{12} \end{Bmatrix}.$$

Its comparison with Eq. (3.5) gives Poisson's ratio ν, shear modulus μ, and Young's modulus E of the graphene as

$$\nu = \frac{\left(\frac{\partial^2 V}{\partial r_{ij}^2}\right)_0 - \frac{B}{8}}{\left(\frac{\partial^2 V}{\partial r_{ij}^2}\right)_0 + \frac{B}{8}}, \quad \mu_{\text{shear}}h = \frac{B}{16\sqrt{3}},$$

$$Eh = \frac{B}{4\sqrt{3}}\frac{\left(\frac{\partial^2 V}{\partial r_{ij}^2}\right)_0}{\left(\frac{\partial^2 V}{\partial r_{ij}^2}\right)_0 + \frac{B}{8}}. \quad (3.7)$$

Here the shear and Young's moduli also appear together with the thickness h, and the subscript "shear" is added to the shear modulus μ in order to distinguish it from the shear modulus to be obtained later from the bending rigidity. For uniaxial stretching ($\varepsilon_{11}\neq 0$, $\varepsilon_{22}=0$), the tension rigidity is

$$\frac{Eh}{1-\nu^2} = \frac{1}{2\sqrt{3}}\left[\left(\frac{\partial^2 V}{\partial r_{ij}^2}\right)_0 + \frac{B}{8}\right].$$

The bending moment is the work conjugate of curvature, and is given by

$$M_{11}+M_{22} = \frac{\sqrt{3}}{2}\left(\frac{\partial V}{\partial \cos\theta_{ijk}}\right)_0 (\kappa_{11}+\kappa_{22}),$$

$$\begin{Bmatrix} M_{11}-M_{22} \\ M_{12} \end{Bmatrix} = 0. \quad (3.8)$$

It has vanishing torsion rigidity (since $M_{12}=0$), and the biaxial bending rigidity [ratio of $(M_{11}+M_{22})$ to $(\kappa_{11}+\kappa_{22})$] is proportional to $(\partial V/\partial \cos\theta_{ijk})_0$, which reflects the multibody atomistic interactions. In other words, a pair potential [$V=V(r_{ij})$] would give vanishing bending stiffness for graphene. The moment-curvature relation (3.8) is different from the classical linear elastic shell theory[39] in the following aspects.

(i) The torque always vanishes, $M_{12}=0$, and the normal components of bending moment always equal, $M_{11}=M_{22}$, such that the graphene can only sustain equibiaxial bending.

(ii) The bending moment is proportional to the sum of principal curvatures $\kappa_{11}+\kappa_{22}$, and is independent of the deviatoric components of curvatures. For example, curvatures $\kappa_{11}=-\kappa_{22}$ give vanishing bending moments.

On the other hand the moment-curvature relation in the classical linear elastic shell theory[39] is

$$M_{11}+M_{22} = \frac{Eh^3}{12(1-\nu)}(\kappa_{11}+\kappa_{22})$$

and

$$\begin{Bmatrix} M_{11}-M_{22} \\ M_{12} \end{Bmatrix} = \frac{\mu h^3}{6}\begin{Bmatrix} \kappa_{11}-\kappa_{22} \\ \kappa_{12} \end{Bmatrix}.$$

Its comparison with Eq. (3.8) gives the biaxial bending rigidity and torsion rigidity as

$$\frac{Eh^3}{12(1-\nu)} = \frac{\sqrt{3}}{2}\left(\frac{\partial V}{\partial \cos\theta_{ijk}}\right)_0, \quad \frac{\mu_{\text{torsion}}h^3}{6} = 0. \quad (3.9)$$

Here the subscript "torsion" is added to the shear modulus μ in order to distinguish it from μ_{shear} above. For unxiaxial curvature ($\kappa_{11}\neq 0$, $\kappa_{22}=0$), the bending rigidity is $(\sqrt{3}/4)\times(\partial V/\partial\cos\theta_{ijk})_0$.

It should be pointed out that the above torsion rigidity, as well as tension, shear, and bending rigidities, are defined for the unstrained equilibrium state of graphene, i.e., infinitesimal strain. It is unintuitive that the torsion rigidity of graphene vanishes. We use a graphene subject only to curvatures κ_{11}, κ_{22}, and κ_{12} to illustrate this. The torsion rigidity is directly proportional to the coefficient of κ_{12}^2 in the Taylor expansion of the energy for each atom $\Phi = \frac{1}{2}\Sigma_{j=1}^3 V(r_{ij};\cos\theta_{ijk}, k\neq i,j)$. With the vanishing in-plane strain $\boldsymbol{\varepsilon}=0$ (and therefore vanishing shift vector $\mathbf{x}=0$), the curvature introduces an out-of-plane displacement field. It can be easily verified the changes of bond length $r_{ij}-r_0$ and angle $\cos\theta_{ijk}+\frac{1}{2}$ are on the order of κ^2 such that all terms associated with the second-order derivatives in the Taylor expansion (2.2) are on the order of $O(\kappa^4)$ and therefore do not contribute to the tension and bending rigidities. Only the term associated with the first-order derivative $\Sigma_{k\neq i,j}(\partial V/\partial\cos\theta_{ijk})_0(\cos\theta_{ijk}+\frac{1}{2})$ in Eq. (2.2) contributes to κ^2. [It is important to recall the other first-order derivative $(\partial V/\partial r_{ij})_0=0$.] For graphene, $(\partial V/\partial\cos\theta_{ijk})_0$ is the same for all bonds, and the κ^2 term becomes $\frac{9}{32}(\partial V/\partial\cos\theta_{ijk})_0 r_0^2(\kappa_{11}+\kappa_{22})(\kappa_{11}+\kappa_{22})$, which depends only on the curvature sum $\kappa_{11}+\kappa_{22}$. Therefore, for the twist curvature κ_{12} or for curvature $\kappa_{11}=-\kappa_{22}$, the κ^2 term vanishes which leads to vanishing torsion rigidity.

Equations (3.5) and (3.8) are constitutive relations for the graphene since they give the force and moment in terms of the in-plane strain and curvature. They are both isotropic even though they give vanishing torsion rigidity. It is unnecessary to define the thickness of graphene unless one wants to determine the stress $\sigma_{\alpha\beta}$ and Young's modulus E from the force $\sigma_{\alpha\beta}h$ and tension rigidity.

IV. THICKNESS OF GRAPHENE

For the classical linear elastic shell theory,[39] the bending rigidity (M_{11}/κ_{11}) is $Eh^3/[12(1-\nu^2)]$ for uniaxial curvature $(\kappa_{22}=0)$, and the tension rigidity $(\sigma_{11}h/\varepsilon_{11})$ is $Eh/(1-\nu^2)$ for uniaxial stretching $(\varepsilon_{22}=0)$. The ratio of bending to tension rigidities is $h^2/12$. It can be easily verified that the ratio of bending rigidity (M_{11}/κ_{11}) to tension rigidity $(\sigma_{11}h/\varepsilon_{11})$ is also $h^2/12$ for uniaxial tension and bending $(\sigma_{22}=0, M_{22}=0)$, equibiaxial stretching and curvature $(\varepsilon_{11}=\varepsilon_{22}, \kappa_{11}=\kappa_{22})$ and for equibiaxial tension and bending $(\sigma_{11}=\sigma_{22}, M_{11}=M_{22})$. It remains the same, $h^2/12$, because the ratio of torsion rigidity to biaxial bending rigidity, $(1-\nu)/(1+\nu)$, is always the same as the ratio of shear to biaxial moduli in the classical linear elastic shell theory.[39] Accordingly, the effective thickness of graphene (or CNTs) has been defined as[4,12,14,22–24]

$$h = \sqrt{\frac{12\ \text{bending rigidity}}{\text{tension rigidity}}}. \quad (4.1)$$

For graphene, the moment-curvature relation (3.8) gives vanishing torsion rigidity but (3.5) gives nonvanishing shear rigidity. Therefore the torsion to bending rigidity ratio, which is zero, is different from the shear to biaxial moduli ratio. For uniaxial stretching $(\varepsilon_{22}=0)$ and curvature $(\kappa_{22}=0)$, the tension rigidity is

$$\frac{1}{2\sqrt{3}}\left[\left(\frac{\partial^2 V}{\partial r_{ij}^2}\right)_0 + \frac{B}{8}\right]$$

and the bending rigidity is

$$\frac{\sqrt{3}}{4}\left(\frac{\partial V}{\partial\cos\theta_{ijk}}\right)_0,$$

which gives the thickness

$$h_{\text{uniaxial stretching}} = 3\sqrt{\frac{2\left(\frac{\partial V}{\partial\cos\theta_{ijk}}\right)_0}{\left(\frac{\partial^2 V}{\partial r_{ij}^2}\right)_0 + \frac{B}{8}}}$$

[which would be zero without the multibody coupling term, $(\partial V/\partial\cos\theta_{ijk})_0=0$]. For equibiaxial stretching $(\varepsilon_{11}=\varepsilon_{22})$ and curvature $(\kappa_{11}=\kappa_{22})$, the thickness becomes

$$h_{\text{equibiaxial stretching}} = 3\sqrt{\frac{2\left(\frac{\partial V}{\partial\cos\theta_{ijk}}\right)_0}{\left(\frac{\partial^2 V}{\partial r_{ij}^2}\right)_0}},$$

while for equibiaxial tension-compression $(\varepsilon_{11}=-\varepsilon_{22}, \kappa_{11}=-\kappa_{22})$, the thickness is zero and the graphene loses its bending rigidity. Therefore, the thickness defined in Eq. (4.1) is not a constant, and it depends on the type of loading. For the proportional biaxial stretching $\varepsilon_{22}=\lambda\varepsilon_{11}$ and curvature $\kappa_{22}=\lambda\kappa_{11}$, the thickness given by Eq. (4.1) becomes

$$h = 3\sqrt{\frac{2\left(\frac{\partial V}{\partial\cos\theta_{ijk}}\right)_0}{\left(\frac{\partial^2 V}{\partial r_{ij}^2}\right)_0 + \frac{1-\lambda}{1+\lambda}\frac{B}{8}}}, \quad (4.2)$$

which clearly depends on the type of loading represented by λ. However, even Eq. (4.2) cannot represent the general loading since it requires the curvature ratio κ_{22}/κ_{11} and strain ratio $\varepsilon_{22}/\varepsilon_{11}$ to be the same.

For the graphene subject to uniaxial tension $(\sigma_{22}=0)$, $\lambda=\varepsilon_{22}/\varepsilon_{11}=-\nu$ $(=\kappa_{22}/\kappa_{11})$, the effective thickness becomes very simple:

TABLE II. Results for gaphene given by the Brenner potential.[a]

	Thickness	Young's modulus	Poisson's ratio
Uniaxial tension	0.0618 nm	3.81 TPa	0.412
Uniaxial stretching	0.0734 nm	3.21 TPa	0.412
Equibiaxial stretching	0.0874 nm	2.69 TPa	0.412

[a]Reference 17.

$$h_{\text{uniaxial tension}} = 3\sqrt{\frac{\left(\frac{\partial V}{\partial \cos\theta_{ijk}}\right)_0}{\left(\frac{\partial^2 V}{\partial r_{ij}^2}\right)_0}}, \tag{4.3}$$

which is about 70% of the thickness for equibiaxial stretching and curvature. However, Eq. (4.3) is for uniaxial tension but not uniaxial bending (i.e., $M_{22} \neq 0$).

It should be emphasized that the tension and bending rigidities in Eqs. (3.7) and (3.9) are well defined, and are independent of the type of loading. The dependence on the type of loading appears only when one wants to define the thickness.

V. RESULTS FOR THE BRENNER POTENTIAL

The Brenner potential[17] is widely used in the atomistic study of CNTs since it gives accurate binding energy and lattice constants of graphite, diamond, simple cubic, and face-centered-cubic carbon, as well as the vacancy formation energy for diamond and graphite. Its five constants and equilibrium bond length are given in Sec. II. Table II gives the thickness [defined in Eq. (4.1)], Young's modulus, and Poisson's ratio of graphene for uniaxial tension, uniaxial stretching, and equibiaxial stretching. The thickness, and therefore Young's modulus, depend on the type of loading, and are therefore not strictly constants, but Poisson's ratio is. The thickness varies from 0.0618 nm to 0.0874 nm, which is consistent with the range of thickness reported in Table I for atomistic simulations together with the shell model.

TABLE III. Results for gaphene given by the second-generation Brenner potential.[a]

	Thickness	Young's modulus	Poisson's ratio
Uniaxial tension	0.0574 nm	4.23 TPa	0.397
Uniaxial stretching	0.0678 nm	3.58 TPa	0.397
Equibiaxial stretching	0.0811 nm	2.99 TPa	0.397

[a]Reference 18.

The second-generation Brenner potential[18] has been developed to improve its agreement with Young's moduli of graphite and diamond, as well as the bond breaking energy. The five constants and equilibrium bond length are also given in Section II. Table III shows the graphene thickness, Young's modulus, and Poisson's ratio. The range of thickness is similar to that in Table II for the Brenner potential, and is also consistent with the range in Table I for atomistic simulations together with the shell model.

Figure 2 shows the graphene thickness h versus λ for both interatomic potentials, where $\lambda = \varepsilon_{22}/\varepsilon_{11} = \kappa_{22}/\kappa_{11}$ represents different type of loading. For equibiaxial tension-compression $\lambda = -1$, the graphene thickness is zero since $\kappa_{11} = -\kappa_{22}$ leads to zero bending moments and therefore vanishing bending rigidity. The thickness reaches the maximum at equibiaxial stretching ($\lambda = 1$). Different types of loading, including the uniaxial tension, are clearly marked in Fig. 2.

Following the same approach we have studied the single-wall CNTs subject to uniaxial tension. Instead of giving the thickness, which depends on the type of loading, we show the well-defined tension rigidity versus the nanotube radius R in Fig. 3 for armchair and zigzag CNTs. For $R > 1$ nm, the tension rigidity is essentially independent of the nanotube radius and chirality, and is the same as that for the graphene. For $R < 1$ nm, the effect of nanotube radius becomes significant, particularly for the second-generation potential,[18]

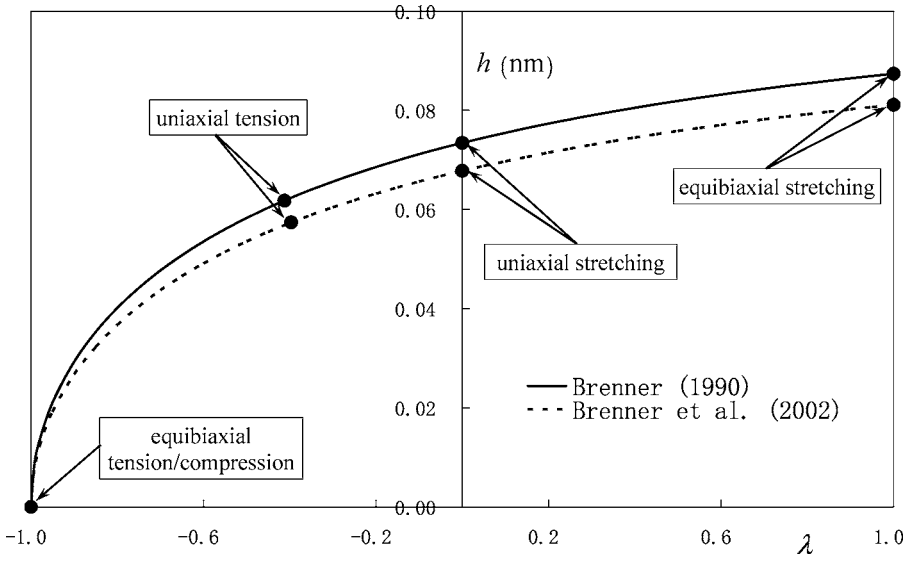

FIG. 2. The effective thickness h of graphene, where $-1 \leqslant \lambda \leqslant 1$ represents different types of loading, including equibiaxial stretching, uniaxial stretching, uniaxial tension, and equibiaxial tension-compression.

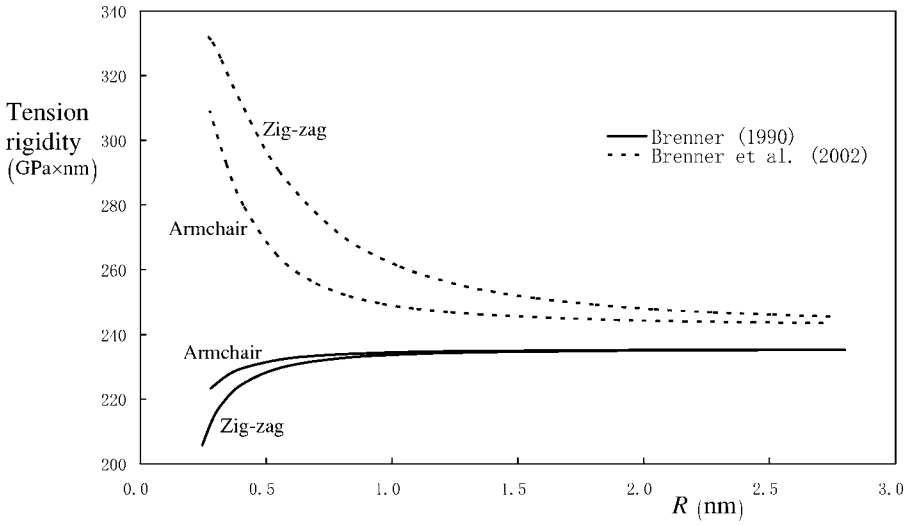

FIG. 3. The tension rigidity of carbon nanotubes versus the nanotube radius R.

which also shows a strong dependence on the CNT chirality (armchair versus zigzag at small CNT radius). It is observed that Brenner's interatomic potential[17] and second-generation potential[18] predict opposite dependence of tension rigidity on the nanotube radius.

VI. DISCUSSION ON "YAKOBSON'S PARADOX"

The well-known "Yakobson's paradox"[33] refers to the contradicting values of Young's modulus reported in the literature for single-wall CNTs. Young's moduli reported in experiments, first-principle calculations, and classical molecular dynamics simulations based on empirical interatomic potentials are around 1 TPa,[33] if the interlayer spacing of graphite, 0.34 nm, is taken as the CNT thickness h. This value is also consistent with Young's modulus of graphite.

Young's modulus of single-wall CNT ropes is 0.81 ± 0.41 TPa reported in experiments and first-principle calculations.[33] Unlike an individual single-wall CNT, a CNT rope consists of many CNTs and can be considered as a three-dimensional bulk solid in the first-principle calculations such that its Young's modulus does not require any assumption of CNT thickness.

Young's moduli of single-wall CNTs reported from the atomistic simulations together with the linear elastic shell model, however, are between 4 and 5 TPa, much higher than those reported above.[33] Here, Young's modulus is obtained by the ratio of well-defined stiffness Eh to the thickness h, where h is obtained from Eq. (4.1) and is not well defined due to its dependence on the type of loading.

In the following we use a simple model to estimate Young's modulus of single-wall CNT ropes. Figure 4 shows a schematic diagram of a single-wall CNT rope consisting of periodically distributed, parallel single-wall CNTs that form a hexagonal pattern. Let R denote the CNT radius, l_0 the center-to-center distance between CNTs, and l_0 is governed by the van der Waals force.[40] For a given strain ε along the CNT axial direction, the net force on each CNT is $2\pi R(Eh)\varepsilon$, where Eh is the well-defined stiffness. The net area per CNT is $(\sqrt{3}/2)l_0^2$. Young's modulus of the single-wall CNT rope is then estimated as $[4\pi R(Eh)]/\sqrt{3}l_0^2$. Equation (3.7) gives $Eh=236$ GPa nm for the Brenner potential.[17] The CNT radius is taken as $R=0.349$ nm for (5,5) armchair CNTs.[41] The center-to-center distance l_0 between CNTs is $l_0=2R+d_{\mathrm{vdW}}$, where d_{vdW} is the distance between CNT walls. For $d_{\mathrm{vdW}}=0$ (neglecting the van der Waals force), Young's modulus of the single-wall CNT rope is 1.23 TPa. For the other limit, d_{vdW} may be estimated by the equilibrium distance between two graphene planes, 0.341 nm. This gives Young's modulus of the single-wall CNT rope 0.554 TPa. These estimates from 0.554 to 1.23 TPa are in the same range with the experimentally reported values 0.81 ± 0.41 TPa.

The very high Young's modulus $4 \sim 5$ TPa reported in the shell model results from the small and not-well-defined thickness. The tension rigidity was obtained from atomistic simulations for a CNT under simple tension ($\sigma_{11} \neq 0, \sigma_{22}=0$).[4] The bending rigidity was obtained by fitting the energy stored in a CNT prior to deformation via the R^{-2} relation,[4] where R is the CNT radius. This corresponds to the special curvature $\kappa_{11}=0$ and $\kappa_{22}=R^{-1}$. For other curvatures or bending moments, the bending rigidity may be quite different.

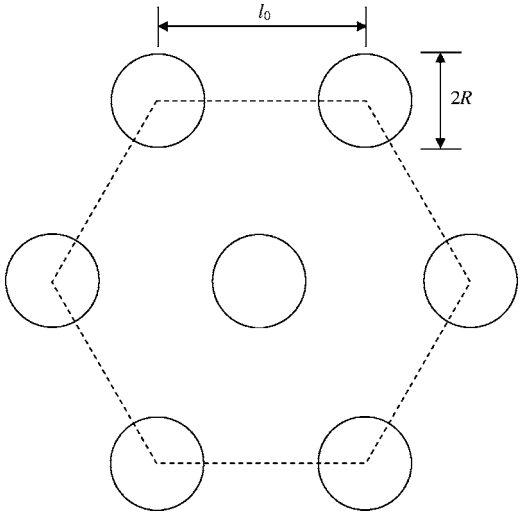

FIG. 4. A schematic diagram of carbon nanotube rope.

VII. CONCLUDING REMARKS

The tension and bending rigidities of graphene and carbon nanotubes (CNT) are obtained analytically such that one can bypass the molecular dynamics simulations to determine them directly from the interatomic potential. The thickness and elastic properties of graphene and CNTs can also be obtained from the interatomic potential. But the thickness, and therefore elastic moduli, also depend on type of loading (e.g., uniaxial tension, uniaxial stretching, equibiaxial stretching), as well as the nanotube radius R and chirality when $R<1$ nm. This dependence on the interatomic potential, loading type, nanotube radius, and chirality explains why the thickness obtained from prior atomistic simulations is scattered. This analytic approach is particularly useful in the study of multi-wall CNTs[23] since their stress state may be complex even under simple loading (e.g., uniaxial tension) due to the van der Waals interactions between nanotube walls.

The present analysis also provides an explanation of Yakobson's paradox.[33] The very high Young's modulus reported from the atomistic simulations together with the shell model may be due to the not-well-defined CNT thickness.

ACKNOWLEDGMENTS

Y.H. acknowledges the supports from the NSF through Nano-CEMMS (Grant No. DMI03-28162) at the University of Illinois and ONR Composites for Marine Structures Program (Grant No. N00014-01-1-0205, program manager Y. D. S. Rajapakse). The authors also acknowledge the supports from the NSFC and Ministry of Education of China.

APPENDIX

The Brenner potential[17] takes the form $V=V_R(r_{ij})-B_{ij}V_A(r_{ij})$, where

$$V_R(r)=\frac{D^{(e)}}{S-1}e^{-\sqrt{2S}\beta(r-R^{(e)})}\cdot f_c(r)$$

and

$$V_A(r)=\frac{D^{(e)}S}{S-1}e^{-\sqrt{2/S}\beta(r-R^{(e)})}\cdot f_c(r)$$

are the repulsive and attractive pair terms (depending only on r). $D^{(e)}=6.00$ eV, $R^{(e)}=0.1390$ nm, $S=1.22$, $\beta=21$ nm^{-1}, f_c is the cutoff function, and the multi-body coupling term B_{ij} is given by

$$B_{ij}=\left[1+\sum_{k(\neq i,j)}G(\theta_{ijk})\right]^{-\delta}.$$

Here

$$G(\theta)=a_0\left[1+\frac{c_0^2}{d_0^2}-\frac{c_0^2}{d_0^2+(1+\cos\theta)^2}\right],$$

$\delta=0.5$, $a_0=0.00020813$, $c_0=330$, and $d_0=3.5$

The equilibrium bond length r_0 can be solved analytically from

$$\left.\frac{\partial V}{\partial r_{ij}}\right|_{r_{ij}=r_0,\theta_{ijk}=120^\circ}=0$$

as

$$r_0=R^{(e)}-\frac{1}{\beta}\frac{\sqrt{S/2}}{(S-1)}\ln B_0, \tag{A1}$$

where B_0 is the multi-body coupling term B_{ij} evaluated at $\theta_{ijk}=120^\circ$, and $B_0=0.96$. The equilibrium bond length is $r_0=0.145$ nm. The other derivatives can be obtained *analytically* as

$$\left(\frac{\partial V}{\partial\cos\theta_{ijk}}\right)_0=\frac{D^{(e)}S}{S-1}\delta a_0c_0^2\frac{1}{(d_0^2+1/4)^2}B_0^{\frac{\delta+1}{\delta}+\frac{1}{S-1}}, \tag{A2}$$

$$\left(\frac{\partial^2 V}{\partial r_{ij}^2}\right)_0=2D^{(e)}\beta^2B_0^{\frac{S}{S-1}}, \tag{A3}$$

$$\left(\frac{\partial^2 V}{\partial r_{ij}\partial\cos\theta_{ijk}}\right)_0=-\frac{D^{(e)}\sqrt{2S}}{S-1}\beta\delta a_0c_0^2\frac{1}{(d_0^2+1/4)^2}B_0^{\frac{\delta+1}{\delta}+\frac{1}{S-1}} \tag{A4}$$

$$\left(\frac{\partial^2 V}{\partial\cos\theta_{ijk}\partial\cos\theta_{ijl}}\right)_0(k\neq l)=-\frac{D^{(e)}S}{S-1}\delta(\delta+1)a_0^2c_0^4\frac{1}{(d_0^2+1/4)^4}B_0^{\frac{\delta+2}{\delta}+\frac{1}{S-1}} \tag{A5}$$

$$\left(\frac{\partial^2 V}{\partial\cos\theta_{ijk}\partial\cos\theta_{ijk}}\right)_0=\frac{D^{(e)}S}{S-1}\delta a_0c_0^2\frac{1}{(d_0^2+1/4)^3}B_0^{\frac{\delta+1}{\delta}+\frac{1}{S-1}}\times\left[2d_0^2-\frac{3}{2}-\frac{(\delta+1)B_0^{\frac{1}{\delta}}a_0c_0^2}{d_0^2+1/4}\right] \tag{A6}$$

*Corresponding author. Electronic address: huang9@uiuc.edu

[1] D. H. Robertson, D. W. Brenner, and J. W. Mintmire, Phys. Rev. B **45**, 12592 (1992).
[2] G. Overney, W. Zhong, and D. Tomanek, Z. Phys. D: At., Mol. Clusters **27**, 93 (1993).
[3] J. M. Molina, S. S. Savinsky, and N. V. Khokhriakov, J. Chem. Phys. **104**, 4652 (1996).
[4] B. I. Yakobson, C. J. Brabec, and J. Bernholc, Phys. Rev. Lett. **76**, 2511 (1996).
[5] C. F. Cornwell and L. T. Wille, Solid State Commun. **101**,

555 (1997).
[6] J. P. Lu, Phys. Rev. Lett. **79**, 1297 (1997).
[7] E. Hernández, C. Goze, P. Bernier, and A. Rubio, Phys. Rev. Lett. **80**, 4502 (1998).
[8] D. Sánchez-Portal, E. Artacho, J. M. Soler, A. Rubio, and P. Ordejon, Phys. Rev. B **59**, 12678 (1999).
[9] E. Hernández, C. Goze, P. Bernier, and A. Rubio, Appl. Phys. A: Mater. Sci. Process. **68**, 287 (1999).
[10] G. V. Lier, C. V. Alsenoy, V. V. Doran, and P. Geerlings, Chem. Phys. Lett. **326**, 181 (2000).
[11] Y. I. Prylutskyy, S. S. Durov, O. V. Ogloblya, E. V. Buzaneva, and P. Scharff, Comput. Mater. Sci. **17**, 352 (2000).
[12] X. Zhou, J. J. Zhou, and Z. C. Ou-Yang, Phys. Rev. B **62**, 13692 (2000).
[13] G. Zhou, W. Duan, and B. Gu, Chem. Phys. Lett. **333**, 344 (2001).
[14] K. N. Kudin, G. E. Scuseria, and B. I. Yakobson, Phys. Rev. B **64**, 235406 (2001).
[15] Y. Jin and F. G. Yuan, Compos. Sci. Technol. **63**, 1507 (2003).
[16] J. Cai, R. F. Bie, X. M. Tan, and C. Lu, Physica B **344**, 99 (2004).
[17] D. W. Brenner, Phys. Rev. B **42**, 9458 (1990).
[18] D. W. Brenner, O. A. Shenderova, J. A. Harrison, S. J. Stuart, B. Ni, and S. B. Sinnott, J. Phys.: Condens. Matter **14**, 783 (2002).
[19] C. H. Xu, C. Z. Wang, C. T. Chan, and K. M. Ho, J. Phys.: Condens. Matter **4**, 6047 (1992).
[20] J. P. Perdew and A. Zunger, Phys. Rev. B **23**, 5048 (1981).
[21] C. Li and T. W. Chou, Int. J. Solids Struct. **40**, 2487 (2003).
[22] Z. C. Tu and Z. C. Ou-Yang, Phys. Rev. B **65**, 233407 (2002).
[23] A. Pantano, D. M. Parks, and M. C. Boyce, J. Mech. Phys. Solids **52**, 789 (2004).
[24] L. Wang, Q. Zheng, J. Z. Liu, and Q. Jiang, Phys. Rev. Lett. **95**, 105501 (2005).
[25] A. Pantano, M. C. Boyce, and D. M. Parks, Phys. Rev. Lett. **91**, 145504 (2004).
[26] C. Q. Ru, J. Appl. Phys. **87**, 7227 (2000).
[27] C. Q. Ru, Phys. Rev. B **62**, 9973 (2000).
[28] M. Arroyo and T. Belytschko, J. Mech. Phys. Solids **50**, 1941 (2002).
[29] G. M. Odegard, T. S. Gates, L. M. Nicholson, and K. E. Wise, Compos. Sci. Technol. **62**, 1869 (2002).
[30] K. I. Tserpes and P. Papanikos, Composites, Part B **36**, 468 (2005).
[31] T. Vodenitcharova and L. C. Zhang, Phys. Rev. B **68**, 165401 (2003).
[32] S. V. Goupalov, Phys. Rev. B **71**, 085420 (2005).
[33] O. A. Shenderova, V. V. Zhirnov, and D. W. Brenner, Crit. Rev. Solid State Mater. Sci. **27**, 227 (2002).
[34] J. Tersoff, Phys. Rev. Lett. **61**, 2879 (1988).
[35] T. Belytschko, S. P. Xiao, G. C. Schatz, and R. Ruoff, Phys. Rev. B **65**, 235430 (2000).
[36] P. Zhang, Y. Huang, P. H. Geubelle, P. A. Klein, and K. C. Hwang, Int. J. Solids Struct. **39**, 3893 (2002).
[37] P. Zhang, H. Jiang, Y. Huang, P. H. Geubelle, and K. C. Hwang, J. Mech. Phys. Solids **52**, 977 (2004).
[38] S. Timoshenko, *Theory of Elasticity* (McGraw-Hill, New York, 1934).
[39] S. Timoshenko, *Theory of Plates and Shells* (McGraw-Hill, New York, 1940).
[40] L. A. Garifalco, M. Hodak, and R. S. Lee, Phys. Rev. B **62**, 13104 (2000).
[41] H. Jiang, P. Zhang, B. Liu, Y. Huang, P. H. Geubelle, H. Gao, and K. C. Hwang, Comput. Mater. Sci. **28**, 429 (2003).